Electronic Supplementary Information (ESI)

Photo–induced magnetic properties of the $[Cu^{II}(bapa)]_2[Mo^{IV}(CN)_8]\cdot 7H_2O$ molecular ribbon

Olaf Stefańczyk,*[a,b,c] Anna M. Majcher,[d] Michał Rams,[d] Wojciech Nitek,[a] Corine Mathonière,*[b,c] and Barbara Sieklucka*[a]

[a] Faculty of Chemistry, Jagiellonian University in Kraków, Ingardena 3, 30–060 Kraków, Poland. E–mail: olaf.stefanczyk@uj.edu.pl, barbara.sieklucka@uj.edu.pl

[b] CNRS, ICMCB, UPR 9048, F–33600 Pessac, France. E–mail: corine.mathoniere@icmcb.cnrs.fr

[c] University Bordeaux, ICMCB, UPR 9048, F–33600 Pessac, France.

[d] Institute of Physics, Jagiellonian University in Kraków, Łojasiewicza 11, 30–348 Kraków, Poland.

Contents

Table S1. Crystal data, data collection, and refinement parameters for **1**.

	1
Formula	$C_{60}H_{118}Cu_6Mo_3N_{42}O_8$
M_r	2225.02
Temp. / K	120(2)
Wavelength / Å	0.71073
Crystal system	Triclinic
Space group	P -1
a / Å	15.5673(6)
b / Å	16.1758(6)
c / Å	24.8869(10)
α / °	102.370(2)
β / °	91.285(2)
γ / °	115.542(2)
V / Å^3	5476.1(4)
Z	2
D_c / Mg·m^{-3}	1.349
μ / mm^{-1}	1.531
F(000)	2272
θ range (°)	0.84 - 26.43
Index ranges	$-19 \le h \le 19$, $-20 \le k \le 20$, $-30 \le l \le 31$
Reflections collected / unique	81409 / 22482 (R_{int} = 0.0382)
Completeness to θ	99.6 % (θ = 26.43°)
Data/restraints/parameters	22482 / 0 / 1072
GOF on F^2	1.122
R_1 / wR_2 (I>2σ(I))	0.0485 / 0.1477
R_1 / wR_2 (all data)	0.0661 / 0.1549
Largest diff. peak and hole / e·Å^{-3}	1.596 / -1.908

Table S2. Selected bond lengths and angles for **1**.

Bond lengths [Å]					
Mo1–C11	2.134(5)	C11–N11	1.150(5)	N11–Cu8	2.027(4)
Mo1–C12	2.159(4)	C12–N12	1.143(5)	N12–Cu6	2.007(3)
Mo1–C13	2.152(4)	C13–N13	1.144(5)	N13–Cu4	2.021(4)
Mo1–C17	2.137(4)	C17–N17	1.140(5)	N17–Cu6	2.149(3)
Mo2–C21	2.160(4)	C21–N21	1.147(5)	N21–Cu5	2.230(4)
Mo2–C22	2.142(4)	C22–N22	1.157(5)	N22–Cu7	2.190(3)
Mo2–C23	2.161(4)	C23–N23	1.147(5)	N23–Cu9	2.051(5)
Mo3–C31	2.165(4)	C31–N31	1.145(5)	N31–Cu4	2.218(3)
Mo3–C33	2.125(5)	C33–N33	1.150(6)	N33–Cu9	1.986(4)
Mo3–C35	2.165(4)	C35–N35	1.139(5)	N35–Cu5	2.029(4)
Mo3–C36	2.137(4)	C36–N36	1.144(5)	N36–Cu8	2.153(4)
Mo3–C37	2.152(4)	C37–N37	1.150(5)	N37–Cu7	2.013(4)

Angles [°]			
Mo1–C11–N11	178.8(4)	C11–N11–Cu8	151.0(4)
Mo1–C12–N12	177.5(4)	C12–N12–Cu6	171.8(3)
Mo1–C13–N13	176.5(4)	C13–N13–Cu4	167.5(4)
Mo1–C17–N17	177.2(4)	C17–N17–Cu6	160.2(3)
Mo2–C21–N21	176.3(3)	C21–N21–Cu5	143.6(3)
Mo2–C22–N22	178.3(3)	C22–N22–Cu7	142.6(3)
Mo2–C23–N23	177.0(3)	C23–N23–Cu9	165.4(3)
Mo3–C31–N31	179.8(4)	C31–N31–Cu4	157.1(3)
Mo3–C33–N33	176.3(4)	C33–N33–Cu9	154.2(4)
Mo3–C35–N35	178.9(4)	C35–N35–Cu5	166.1(4)
Mo3–C36–N36	179.0(4)	C36–N36–Cu8	158.1(4)
Mo3–C37–N37	176.1(4)	C37–N37–Cu7	166.1(4)

Table S3. Results of continuous shape measures analysis for the Mo^{IV} centres.

Geometry	SBTP	SSAPR	STDD
ideal BTP–8	0.000	2.262	2.709
ideal SAPR–8	2.262	0.000	2.848
ideal TDD–8	2.709	2.848	0.000
[Mo1(CN)8]	0.901	1.320	1.352
[Mo2(CN)8]	1.409	0.815	0.915
[Mo3(CN)8]	1.712	0.417	1.562

S_{BTP} – the shape measure relative to the bicapped trigonal prism; S_{SAPR} – the shape measure relative to the square antiprism; S_{TDD} – the shape measure relative to the triangular dodecahedron; a smaller S – value reflects a better match with the ideal geometry ($S = 0$).

Table S4. Results of continuous shape measures analysis for the Cu^{II} centres.

Geometry	S_{TBPY}	S_{SPY}	S_{vOC}
ideal TBPY–5	0.000	5.384	7.342
ideal SPY–5	5.384	0.000	1.741
ideal vOC–5	7.342	1.741	0.000
[Cu1$(NC)_2$(bapa)]	4.106	0.525	1.148
[Cu2$(NC)_2$(bapa)]	5.575	0.528	1.081
[Cu3$(NC)_2$(bapa)]	3.776	0.669	1189
[Cu4$(NC)_2$(bapa)]	5.408	0.606	0.892
[Cu5$(NC)_2$(bapa)]	5.412	0.530	1.004
[Cu6$(NC)_2$(bapa)]	4.844	0.301	1.157

S_{TBPY} – the shape measure relative to the trigonal bipyramide; S_{SPY} – the shape measure relative to the square pyramid; S_{vOC} – the shape measure relative to the vacant octahedron; a smaller S – value reflects a better match with the ideal geometry ($S = 0$).

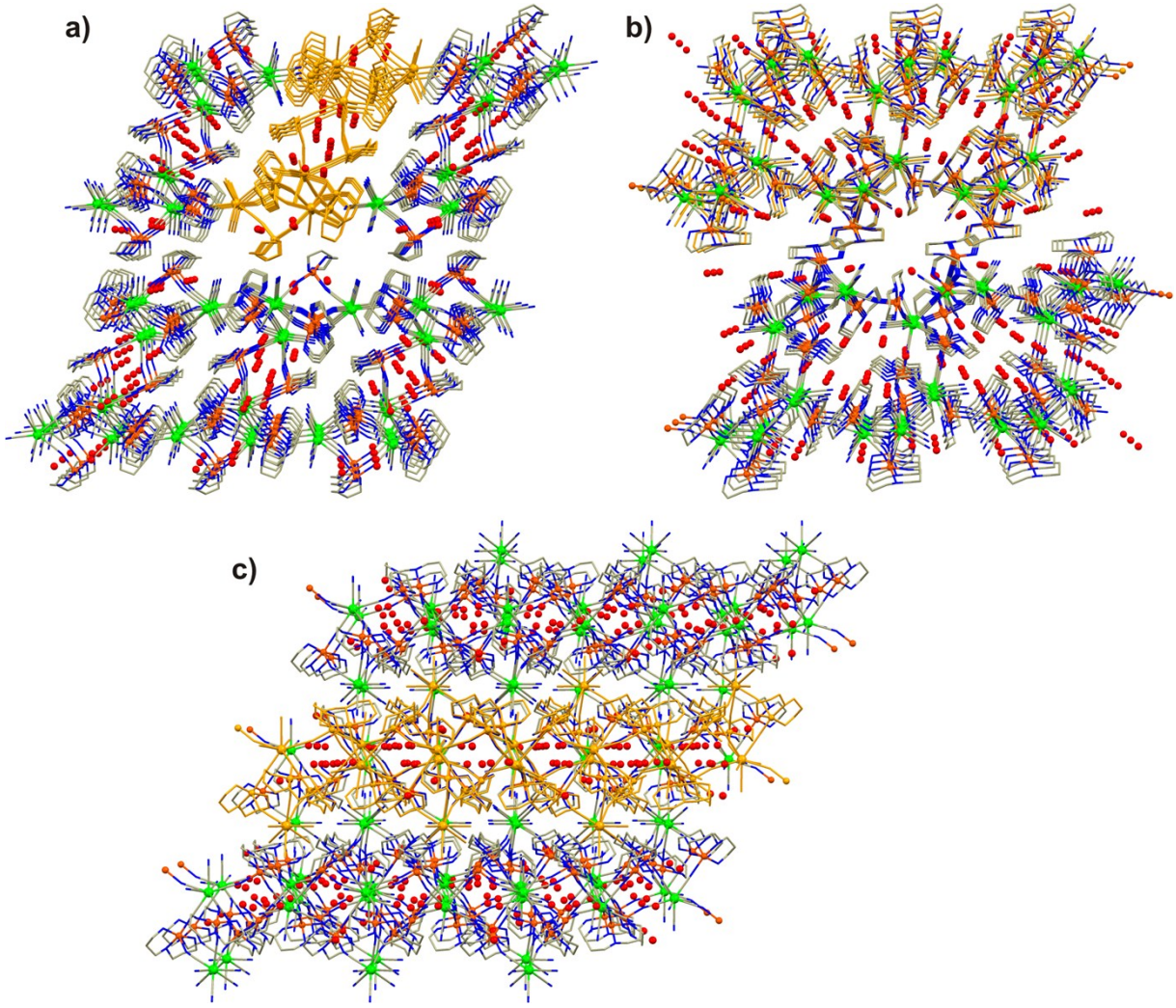

Figure S1. Crystal packing in the structure of **1** along the a – axis (**a**), the b – axis (**b**) and the c – axis (**c**) completed with localized crystallization water molecules (red balls) and with a marked single ribbon (orange). Hydrogen atoms were omitted for clarity.

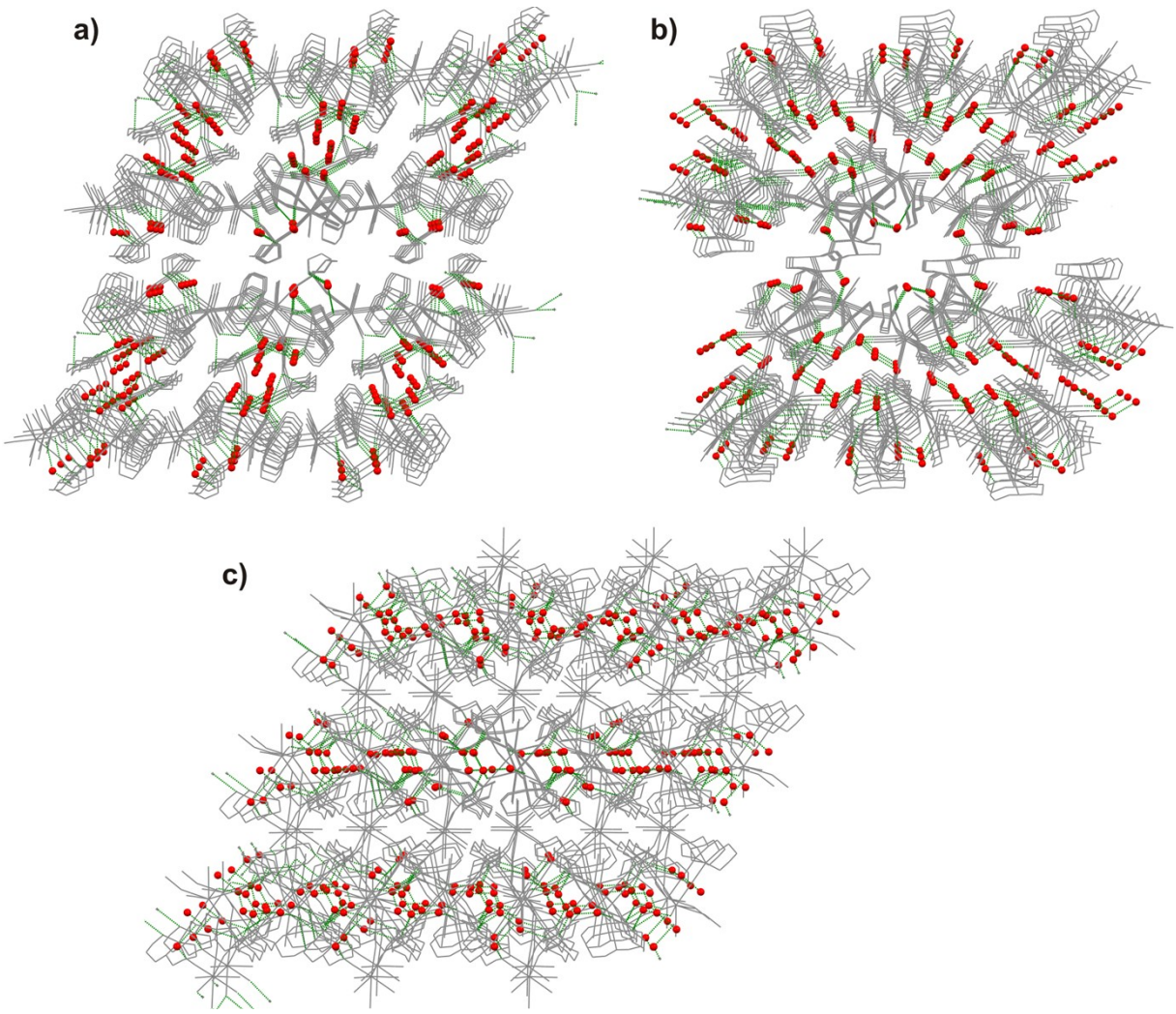

Figure S2. Hydrogen bonds network of **1** (green dashed lines) in crystallographic directions (100) (**a**), (010) (**b**) and (001) (**c**). Hydrogen atoms were omitted for clarity.

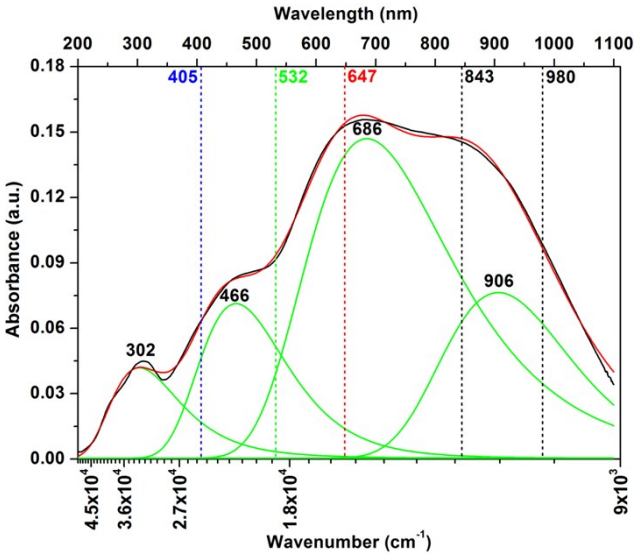

Figure S3. Solid state UV–Vis–NIR absorption spectrum of **1** at room temperature (black line) and a Gaussian deconvolution of the experimental spectrum (green and red lines). Dashed lines represent the wavelengths used for photomagnetic studies.

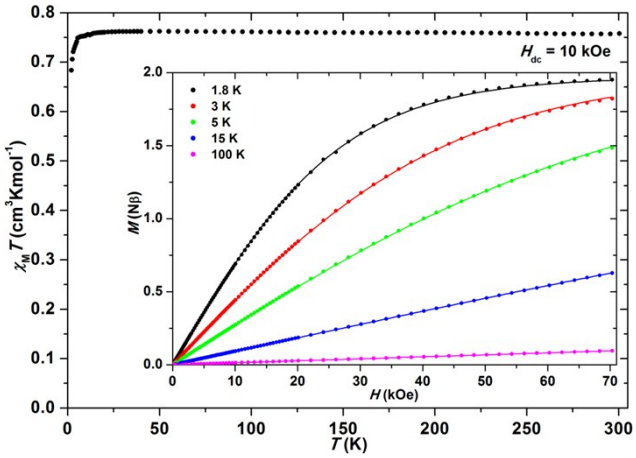

Figure S4. The $\chi_M T(T)$ plot for **1**. **Inset**: $M(H)$ plots for **1** measured at different temperatures (symbols) and Brillouin function fits (solid lines).

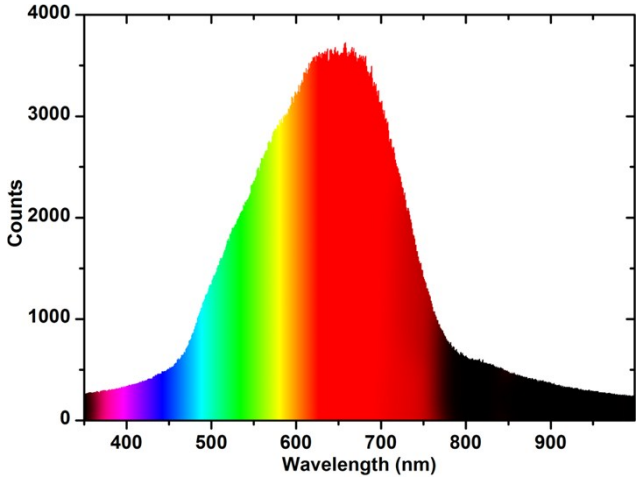

Figure S5. White light spectrum applied in the excitation experiments.

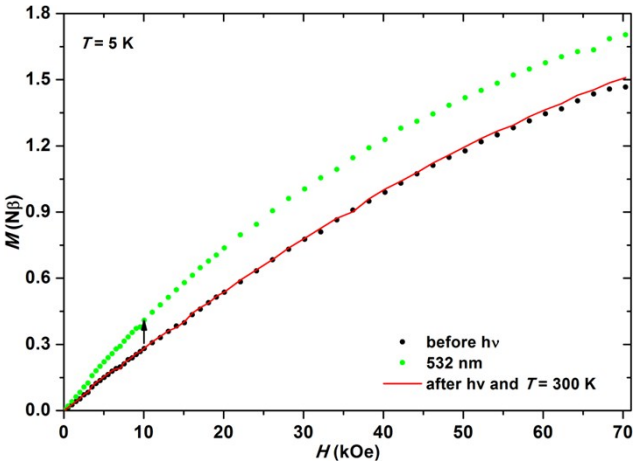

Figure S6. The $M(H)$ plot at 5 K for **1** before and after excitation with 532 nm laser line, and after heating to 300 K.

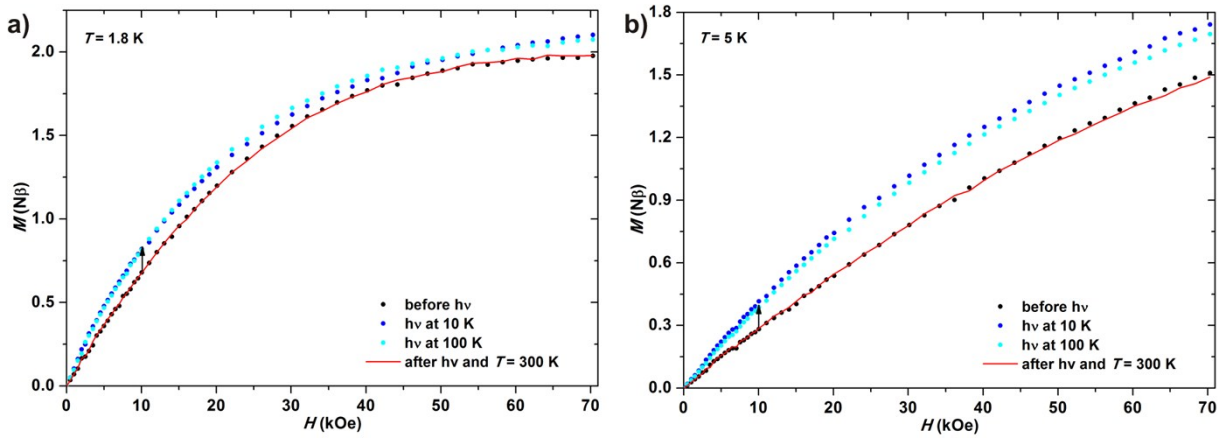

Figure S7. The $M(H)$ plots at 1.8 (**a**) and 5 K (**b**) for **1** before and after excitations with 405 nm laser line performed at T = 10 and 100 K, and after heating to 300 K with a sweep rate of 0.4 K/min.

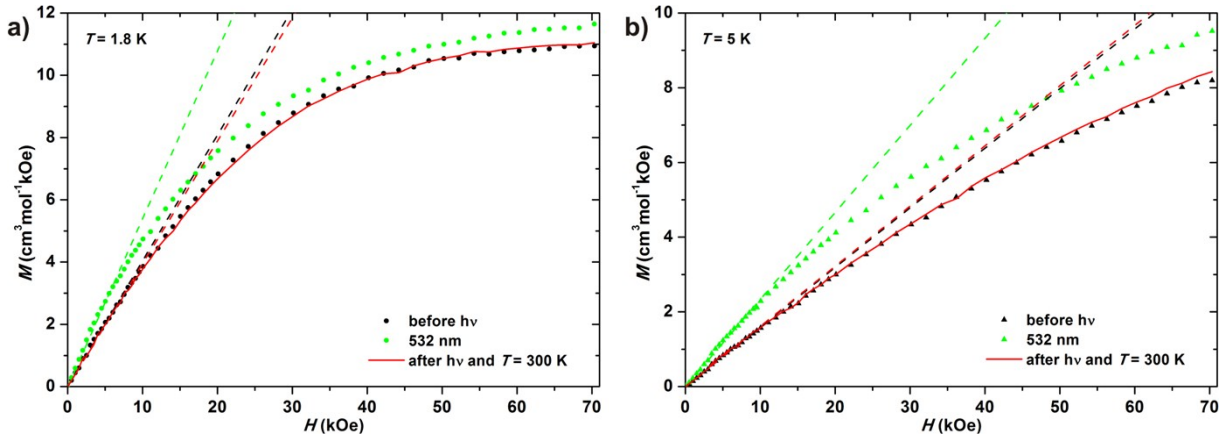

Figure S8. The $M(H)$ plot at 1.8 (**a**) and 5 K (**b**) for **1** before and after excitation with 532 nm laser line, and after heating to 300 K. Dashed lines represent linear fits in the low field (H < 5 kOe) region. It can be clearly seen that $M(H)$ after irradiation is changed not only in the intensity of the signal, but also in the shape of the curves. To emphasize the consistency of our results, we performed a linear fit within the low magnetic field regime to extract the χ_M susceptibilities. The obtained values of the slope before irradiation and after irradiation are in full agreement with the chi values obtained from the $\chi_M T$ vs. T plots.

Table S5. Comparison of the magnetic susceptibility of **1** obtained by different methods at two temperatures before and after excitation with 532 nm laser line, and after heating to 300 K.

	T (K)	χ_M (cm^3mol^{-1}) [a]	χ_M (cm^3mol^{-1}) [b]
before hν	1.8	0.40	0.38
after hν		0.54	0.51
after hν and T = 300 K		0.40	0.38
before hν	5	0.16	0.15
after hν		0.23	0.23
after hν and T = 300 K		0.16	0.15

[a] Values estimated from linear fit to $M(H)$ plots in low magnetic field regime (H < 5 kOe). [b] Values obtained from direct measurements.